An integrated image processing approach to alteration mapping for possible mineralisation in parts of North Central Nigeria using ASTER multispectral data.

D.O. Nnebedum, I.A Oha*, I.A. Okonkwo

Department of Geology, University of Nigeria Nsukka, Enugu State Nigeria

*Corresponding author address: ifeanyi.oha@unn.edu.ng

ORCID: 0000-0002-5465-2114

Abstract - The Keffi area in northcentral Nigeria is characterised by a prominent pegmatitic belt that is closely associated with Pan-African granites. Some of these pegmatites are mineralised and are known to host tin-niobium-tantalum metals and gemstones. The mineralisation is closely associated with ferric-silica-kaolinite type alteration patterns that have been mapped mainly using geochemical tools. This contribution employed a combination of band ratio composition (BRC) and principal component analysis (PCA) to map the alteration type and distribution over an Advanced Spaceborne Thermal Emission and Reflection Radiometer (ASTER) scene. BRC projecting ratio B4/B3 in red, ratio B5+B7/B6 in green and B13/B10 in blue, yielded alteration patterns for ferric, muscovite, and silica zones. Large contrast in eigenvector loadings of covariance PCA in feature selected bands was instrumental in selecting the most suitable PC combination. Bands 1,3,4,5 were selected for PCA targeting ferric oxide and PC2 with sign inversion mapped the ferric oxide content in a single band. Bands 1,4,6,7 were selected for PCA targeting Al-OH bearing minerals and PC3 was identified for hydroxyl mapping. Bands 10,11,12,14 were selected for PCA targeting silica rich material and PC4, with sign inversion, mapped the silica content. RGB Composite generated from ferric_PC2 with sign inversion, Al-OH_PC3 and Silica_PC4 with sign inversion mapped the mineralised zone associated with the complex pegmatites which hosts the gemstones and rare-metals in the study area as shown by field validation. The study demonstrates the usability of Aster data to map alteration patterns around the Keffi area in northcentral Nigeria that are closely associated with the complex pegmatites that hosts gemstones and rare-metal mineralisation within the study area.

Key words: ASTER, Band Ratio, Principal Component Analysis (PCA), Crosta Technique, Mineralization, Alteration.

1.0 Introduction

The Advanced Spaceborne Thermal Emission and Reflection Radiometer (ASTER) is a multispectral imaging system that consists of visible-near-infrared (VNIR), short-wave infrared (SWIR) and thermal infrared (TIR) channels in 14 bands. It was launched in December 1999 onboard NASA's Terra Spacecraft. The ASTER System offers substantial advantages over most available multispectral systems in terms of availability and resolution. Its superior spectral resolution of 6 shortwave infrared (SWIR) bands makes it possible to identify and map minerals and mineral groups such as iron-oxides, carbonates, clays and silica hence amplifying its usefulness in alteration studies. The use of ASTER multispectral data to map mineral alteration is well known and has been documented in different parts of the World [1 – 3]. Band Ratio and combination Technique on ASTER multispectral data has been utilised to identify alteration associated with ferric iron oxides mineral group like haematite, goethite as well as the Al-OH mineral group like koalinite, illite etc [4 – 10]. Principal Component Analysis (PCA) on ASTER bands has been used to delineate alteration zones and different mineralisation styles [2, 11, 12]. In this study, a combination of Band Ratio and PCA techniques are utilised to map mineralisation in parts of northcentral Nigeria where such techniques are yet to be deployed. The motivation for this study is based on the existence of various mineralisation styles that can be recognised by their alteration patterns deducable by the techniques applied.

2.1 Geological setting

Northcentral Nigeria is predominantly underlain by rocks belonging to the Precambrian Basement Complex of Nigeria. They are polycyclic and are known to have been affected by at least four major Orogenic events. They include the Liberian (2700±200Ma), Eburnean (2000±200Ma), Kibaran

(1100±200Ma), and Pan-African (600±150Ma) [13 – 15]. Four major groups of rocks were recognised by [16] in the Basement Complex of Northern Nigeria, they are (i) an underlying high amphibolite facies complex of quartzo-felspathic biotite and hornblende gneiss, migmatites and high-grade metasedimentary relics comprising of older, metasediments. (ii) A supracrustal cover of low to medium grade meta-sediments. (iii) A suit of post syntectonic to late syntectonic Pan-African granitoids also known as the Older Granites. This intrudes the crystalline complex and the supracrustal cover. (iv) Volcanic rocks belonging to the Post Pan-African episode of high-level magmatic activity. The gneisses and migmatitic gneisses complex are the oldest rock units in the Precambrian basement complex and makes up about 60% of the surface area of the Nigerian basement [17]. The rocks consist of gneisses, migmatitc banded gneisses, Augen (characterised by eye shaped feldspar porphyroblasts) or/and porphryoblastic gneisses. The schist belt comprises of low-grade metasediment-dominated belts which trends in a dominant NNE-SSW direction. During the Pan African Orogeny, the schist belt was folded steeply along the basement complex and are considered as relicts of a single supercrustal cover by [16 and 18]. The granitoids have been emplaced within both the Migmatite Gneiss Complex and the Schist Belts, and they occur in all parts of the Nigerian Basement Complex. However, the extent of the Pan-African plutonism had not been fully understood [17].

The Younger granites comprise a distinctive series of alkali felspar granites associated with rhyolites, minor gabbros and syenites. They were first described by [19] as cross-cutting undeformed, post-tectonic alkali granites containing riebeckite or biotite characterised by chilled margins against the country rock. They occur in most cases as sub-volcanic intrusive complexes, as ring dykes and related annular and cylindrical intrusions forming a roughly N-S trending structure which has been traced from northern Africa to the banks of the River Benue at Afu. The Younger granites consist of lithologic units which include, biotite granites, riebeckite granites, riebeckite - biotite granite and hornblende - biotite granite. Other rocks which make up the suite include gabbros, diorites and syenites, with significant volumes of rhyolite (lavas), rhyolitic tuffs. Pegmatites occur widespread in northcentral Nigerian Basement Complex. They are mainly holocrystalline with grain size sometimes in excess of 5cm. The Pegmatites are mainly of the Lithium-Caesium-Tantalum (LCT) type. They comprise both of simple and complex pegmatites with known deposits of gemstones and rare metal mineralisation [20]. Basic intrusives occur mainly as dolerite dykes while rhyolite porphyries are common towards the margins of the north-central basement complex around Nassarawa -Eggon and Gboko areas. Figure 1 shows the geological map of the study area.

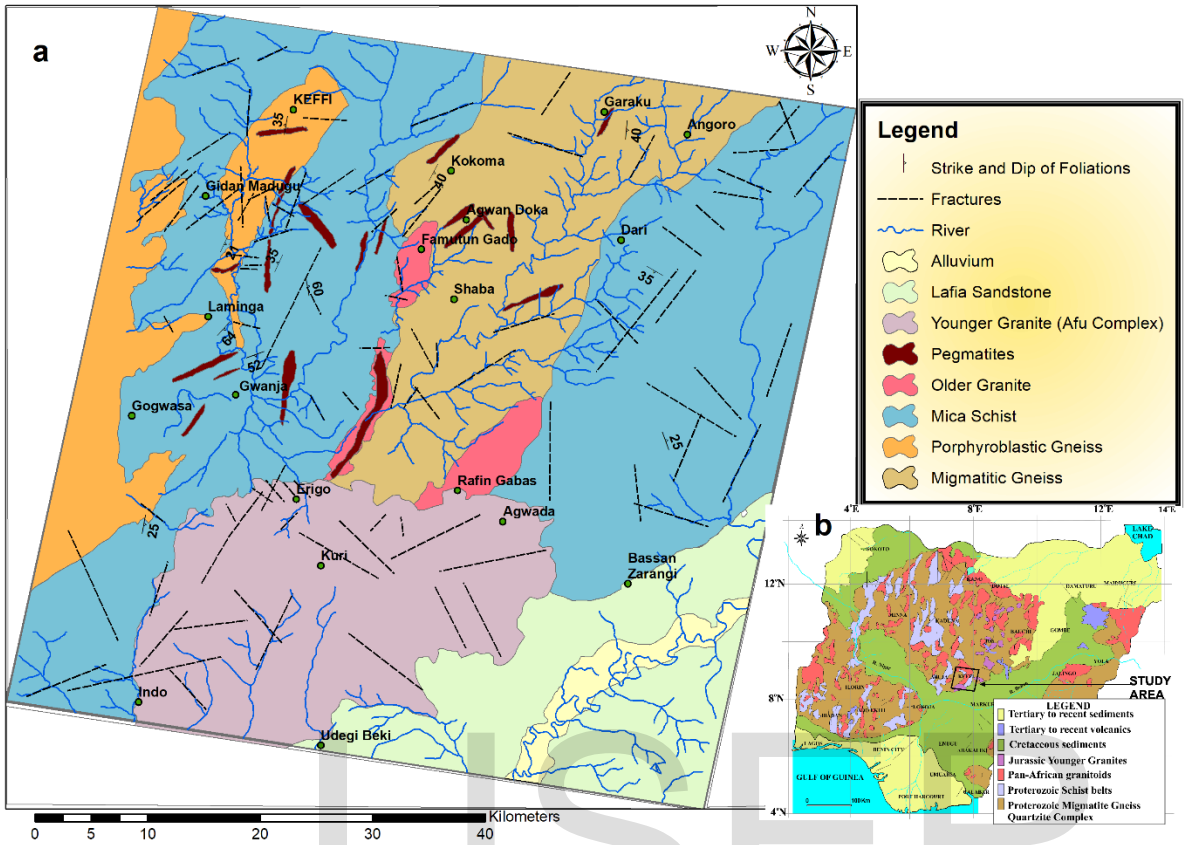

Figure 1: (a) Geological map of the study area (b) Generalised geological map of Nigeria Showing the location of the study area.

3.0 Material and Method

3.1 ASTER Spectral Analysis

The ASTER data used in this study was obtained from the USGS Earth-Data platform accessed through the Earth Explorer website. It consists of one full cloud-free level 1T ASTER scene which covered a part of northcentral Nigeria. The scene is a 60km by 60km multispectral image acquired on February 13, 2007.

The AST_L1T data used for this study utilised the appended radiometric and geometric corrections in the raw AST-L1A product. ASTER bands from the three subsystems were resampled to correspond to the VNIR 15-m spatial dimensions.

Table 1 ASTER Product Specification

ASTER SPECIFICATION					
Instrument Subsystems	Bands	Wavelength (μm)	Spatial Resolution (m)	Swath width (Km)	Signal (bits).
VNIR Visible and Near Infrared	1 2 3N 3B	0.520 – 0.600 0.630 – 0.690 0.760 – 0.860 0.760 – 0.860	15	60	8
SWIR Shortwave Infrared	4 5 6 7 8 9	1.600 – 1.700 2.145 – 2.185 2.185 – 2.225 2.235 – 2.285 2.295 – 2.365 2.360 – 2.430	30	60	8

TIR Thermal Infrared	10 11 12 13 14	8.125 – 8.475 8.475 – 8.825 8.925 – 9.275 10.25 – 10.95 10.95 – 11.65	90	60	12
ORBIT INFORMATION					
Orbit	Orbit Period		Repeat Cycle	Inclination	Altitude
Sun Synchronous Descending	98.9 minutes		16 days	98.2° ± 0.15°	705Km (At equator)

North Central Nigeria is within the semi-arid regions, and the spectral reflectance of rocks and minerals here would be suitable for direct inference of lithology and alteration zones [21, 22]. Several authors [10, 9, 8, 4] showed that mineral groups associated with hydrothermal alterations can be mapped using ASTER data. The possibility of this is based on the fact that the characteristic absorption and radiance features caused by OH, Si-O and other hydroxyl bonds like Mg-OH, Al-OH are within the Shortwave Infrared [23, 3 22]. Figure 2 shows the spectra of selected minerals associated with altered rocks in the study area. The absorption feature observed in the spectra in relation to their reflectance forms the basis for the band combinations carried out in the present study. As can be observed, (fig. 2), ferric iron mineral group mostly have their absorption feature within the Visible and Near Infrared (VNIR) range.

3.2 Band Ratios and Combination

Band ratio (BR) involves the division of the DN value of one band with another to enhance or suppress certain features. These ratios can be combined to form colour composites which further highlights diagnostic features. Band ratio techniques are especially useful in highlighting features that otherwise would have been difficult to identify from raw bands [2]. The technique is generally accepted in geological mapping [24, 7, 22, 2, 4]. Band Ratios that will highlight ferric iron and the hydroxyl mineral group would be useful in mapping mineralised zones based since the zones of mineralisation in the study area are associated with high ferric, silica and Al-OH minerals. Band ratios shown in Table 2 were calculated to highlight the ferric oxide content (B4/B3), silica index (B13/B10) and Al-OH (B5+B7/B6). Fig 3 shows why (B5+B7)/B6 is preferred for this study over B5/B7 for mapping Aluminium Hydroxyl (Al-OH) mineral group due to the granitic composition (Fig. 6) of the pegmatites. The silica index ratio – B13/B10, according to [4] is suitable for mapping silica-rich (quartz) sediments (e.g., quartzites); silicification and silcretes; and quartz veins. B3 – B7, B10 and B13 were designated for ASTER bands 3- 7, 10 and 13, respectively. RGB composite of B4/B3 for ferric oxide content, (B5+B7)/B6 for Al-OH bearing minerals and B13/B10 for silica-rich material mapping was performed to segregate the mineralised zones.

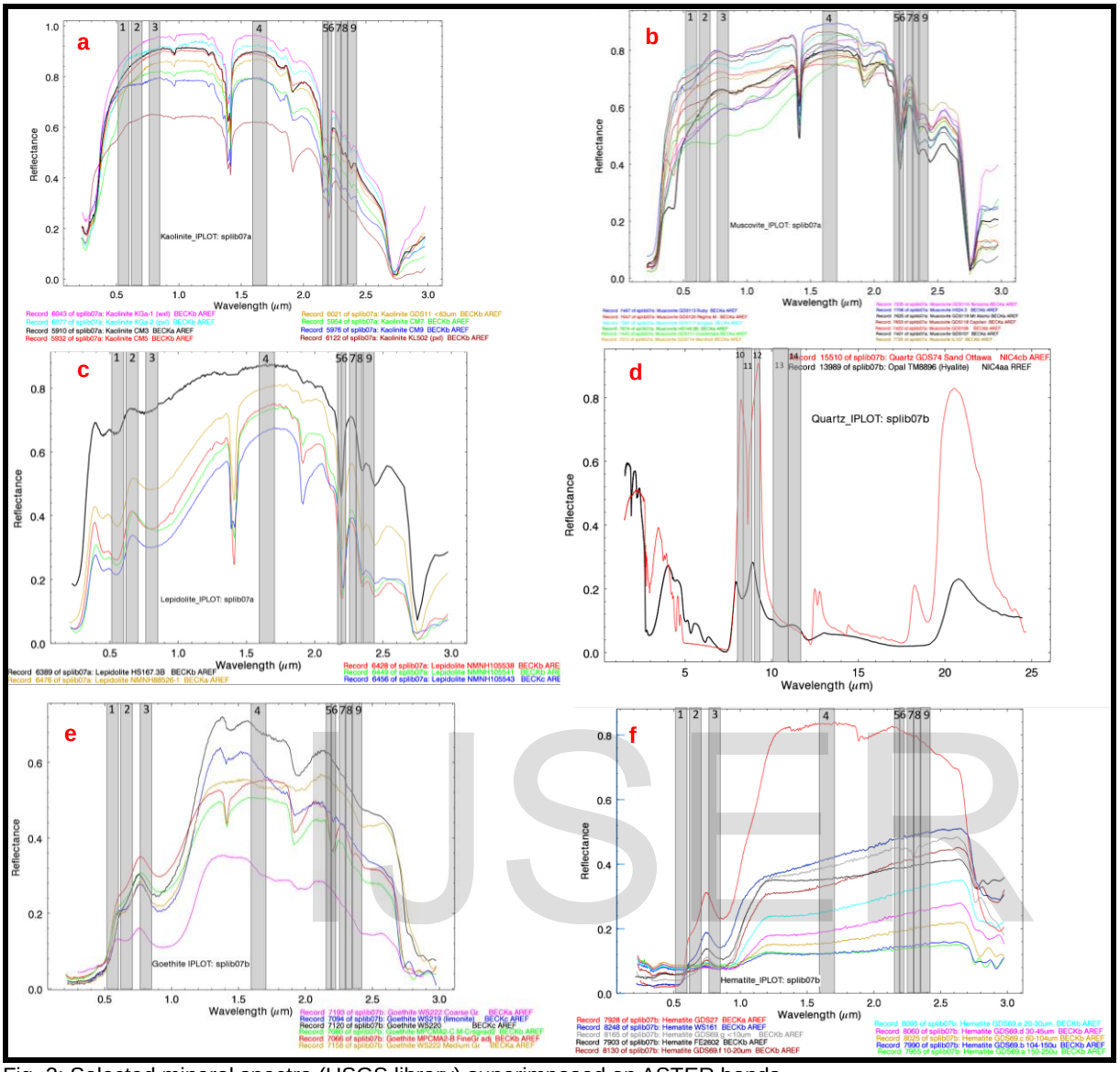

Fig. 2: Selected mineral spectra (USGS library) superimposed on ASTER bands.

Table 2 Band Ratios used in the study.

S/N	Band Ratio	Feature	Comment	Reference
1	B4/B3	Ferric oxide content	hematite, goethite, jarosite	[6], [4]
2	B13/B10	Silica (SiO2 index)	Si-rich (SiO2) units such as quartz, feldspars, Al-clays	[2], [8]
3	(B5+B7)/B6	Al-OH content	phengite, muscovite, kaolinite, illite, lepidolite, paragonite, montmorillonite, beidellite, dickite, brammalite	[9], [6], [4], [5].

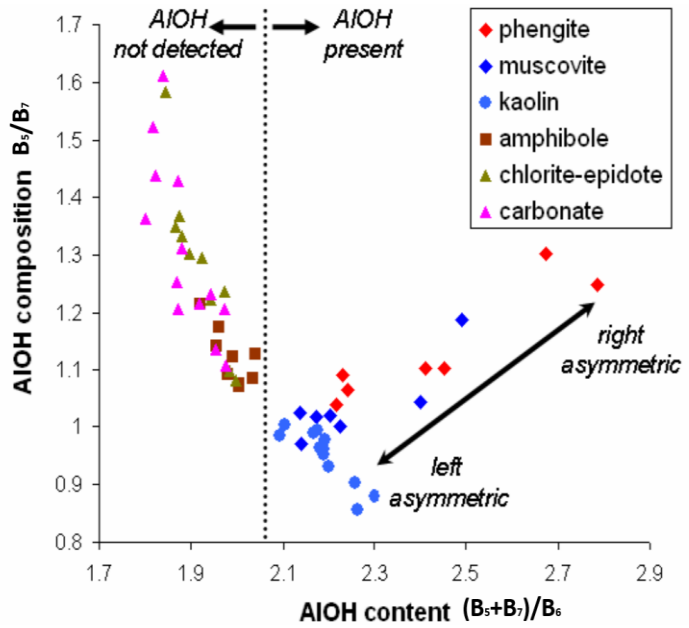

Fig 3 Scattergram of the ASTER derived "Al-OH content" versus the "Al-OH composition" [6].

3.3 Principal Component Analysis

Principal Component Analysis (PCA) is a multivariate statistical technique that selects uncorrelated linear combinations of variables in such a way that each component successively extracted has linear combination and a smaller variance [25, 26, 2]. In simple terms, PCA is a technique that identifies patterns in data, accentuating its similarities and differences by displaying the greatest variance on the first axis called Principal Component [27]. The second-largest variance is displayed on the second axis that is orthogonal to the first, and so on. PCA is very useful in suppressing irradiance paraphernalia that are common in all bands of multispectral data in order to highlight spectral reflectance features of surface materials which have geological relevance [12, 28]. Each array of PC images is a display of the sum of the products of eigenvectors and corresponding Digital Number (DN) values for spectral bands of the original data at each pixel [27]. Therefore, the DN value in the PC image depends upon the magnitude and sign of the eigenvectors together with DN values in the input image.

PCA techniques has been successfully applied on Landsat TM, in mapping iron oxide/hydroxides associated with sulfide ore bodies in granite-greenstone belt terrains [28]. The technique applied utilised the relationship between eigenvector loading and the spectral responses of the ferric oxide rich soils to segregate the zones of the sulfide ore bodies. This technique was termed feature-orientated principal component selection (FPCS). [30] was able to map the spectral information associated with alteration minerals into a single PC using the Landsat TM. In his procedure, Landsat bands 1, 3, 4, and 5 were used to map spectral information of ferric oxide/hydroxide into PC3 or PC4 while for hydroxyl bearing minerals and carbonates, bands 1, 4, 5, and 7 were utilised. Feature oriented Principal Component Selection has been deployed successfully in mineral exploration [11, 12, 31, 32]. In South American regions with sparse or no vegetation, this technique has become a routine tool for alteration mapping using Landsat TM [11, 12].

[11] successfully used the adapted form of the "Crosta Technique" proposed by [30] in targeting alteration minerals (kaolinite, illite and alunite) associated with epithermal deposits in Patagonia, Argentina. The technique is similar to that of [30] where the PC containing the spectral information of interest shows highest eigenvector loading from the ASTER bands coinciding with the targets most diagnostic absorption features, irrespective of the sign in the eigenvector matrix. Isolating the PC with eigenvector loading for target minerals and generating a composite out of these PC's, kaolinite, illite and alunite clusters were mapped, and the results were confirmed by field spectroscopy.

PCA tends to segregate the spectral information of target mineral/mineral group into a single band upon selection of the appropriate bands related to the absorption feature of the minerals [11, 12, 30]. The FPCS technique adapted by [11], two reflection and absorption bands each are selected for the PC analysis. Higher eigenvector loadings with large contrast between the major reflectance and absorption bands gives a clue choice PC most likely to discriminate the target mineral group, irrespective of their sign convention

[11, 12, 27].

In this study, the target mineral groups are ferric oxide/hydroxide, hydroxyl bearing minerals and the quartz-rich materials. In discriminating the suitable bands for PCA in this study, reflectance curves of target minerals displayed in Fig. 2 were examined. Sequel to this, bands 1, 3, 4 and 5 were selected for the Ferric oxide/hydroxide target. Bands 1 and 3 are the absorption bands while Bands 4 and 5 are the reflectance bands. ASTER bands 1, 4, 6, and 7 [11] were selected for the hydroxyl bearing materials (Table 3). Bands 1 and 6 are the absorption bands for the Kaolinite rich hydroxyl bearing materials while bands 4 and 7 are the reflectance bands. For the Silica-rich materials, TIR bands – 10, 11, 12 and 14 were selected where 10 and 12 are reflectance bands whereas bands 11 and 14 constitute the absorption bands.

Table 3. Selected Bands for Principal Component Analysis

	Key Minerals associated with mineralisation		
	Ferric iron (Loughlin, 1991)	**Al-OH** Kaolinite (Crosta et al, 2003)	**Silica**
ASTER Bands	1	1	10
	3	4	11
	4	6	12
	5	7	14

4. Results, Analyses, and Discussion

4.1 Band Ratio Analysis

Band ratio analysis generated image (Fig 4) that reveals alteration patterns/mineralised zones related to ferric oxide, hydroxyl (Al-OH) minerals and silica-rich materials. RGB composite of ferric oxide, Al-OH and Silica ratios is given in Fig 4a. Zones with whitish colouration are areas with high content of ferric, Al-OH, silica-rich materials. Field validation confirms the above claims (Fig. 4c) as the whitish shades are suggestive of high prospective zones for gemstones and rare metals mineralisation.

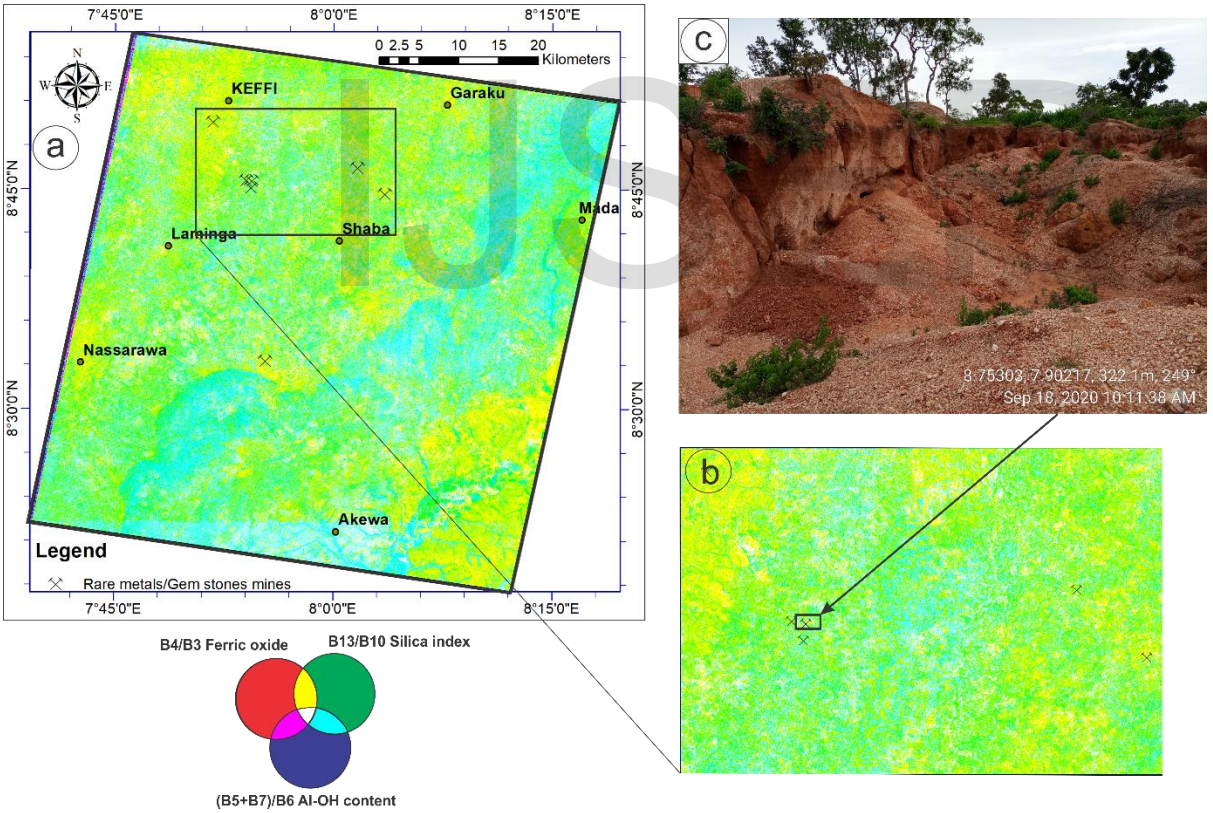

Fig. 4(a): Band Ratio Composite (BRC) of B4/B3_Ferric oxide in red, B13/B10_silica index in green and B5+B7/B6_Al-OH content in blue. (b):Subset showing mineralized areas in pale yellow and white shades. (c) Field validation of one of the targets in fig. 4b showing open pit excavation with pronounced ferric oxide and silica alteration.

4.2 Principal Component Analyses

The statistical results shown in Table 4 display the eigenvector matrix of PC calculation for the selected bands. For silica-rich materials, PC1 showed moderate eigenvector loadings in negative sign. The loadings for all the selected bands are moderate except Band 14 which manifest slightly higher eigenvector loading (-0.60586). Obviously, the contrast between the reflectance and absorption bands will be small irrespective of sign inversion. This eliminates PC1 as

a choice for mapping silica. PC2 showed fairly large contrast between the refection bands (band 10: 0.244556; band 12: 0.343224) and absorption bands (band 11: 0.44728; band 14: -0.78888) although the eigenvector loading is low to moderate. PC2 may be considered for silica index mapping because at Band 12 (reflectance band) the eigenvector is low to moderate (0.34322) while Band 14 (reflectance band) possesses a high negative value (-0.78888). Its contrast is fairly good. PC3 showed high eigenvector loading for the reflectance bands (band 10: 0.795894; band 12: -0.60134) but near-zero eigenvector loadings for the absorption bands. Near zero eigenvector loadings constitutes noise [2, 33]. PC4 of the TIR selected bands showed high and positive eigenvector loadings at band 11 (0.764066) and high but negative at band 12 (-0.53548). Silica spectral curve in Fig 2d shows that silica has absorption in band 11 and high reflectance in band 12. As a result, PC with high and negative eigenvector for band 11 as well as high and positive eigenvector for band 12 will provide good contrast for silica mapping into a single image. In the case of PC4 a sign inversion will be required to achieve this condition. This portrays PC4 as a better choice than PC2 for silica segregation.

The eigenvector statistics of the PCA calculated for the ferric selection bands are shown in Table 4. PC 1 has moderate to high eigenvector loading with all positive signs. This PC will not allow for better contrast between the reflectance and absorption bands required to properly discriminate the ferric iron/oxide content [11] and consequently will not be a choice PC for ferric mapping. In PC2, band 1, an absorption band for ferric minerals (Fig 2 e & f), displayed an approximately high eigenvector loading (0.498953) with a positive sign. Band 5, a reflection band showed high and negative eigenvector value (-0.73974). Low to moderate eigenvector loadings were experienced for band 3 (0.323076) and band 4 (-0.31535). This PC will serve as good candidate for ferric mapping based the high values of the eigenvectors in the absorption and reflectance bands but will require a sign inversion to reflect the low values at absorption and high values at reflectance band.

PC 3 gave moderate and positive values at band 1 and band 5; moderate negative loading was observed in band 3, while band 4 shows high and negative loading. Upon sign inversion, PC3 can be a candidate for ferric iron/oxide mapping. In the absorption bands, PC 4 has relatively low and negative eigenvector loading in band 1 (-0.32513) while band 3 has high and positive value (0.733875). For the reflectance bands, PC4 shows high and negative value in band 4 (-0.50541) whereas in band 5, a relatively low and positive value is observed (-0.316667). Considering the eigenvector loadings for the best contrast in the reflectance and absorption bands, PC2 upon sign inversion, appears to be the best PC for mapping ferric iron/oxide content in a single band.

The result of the eigenvector statistics calculated for hydroxyl bearing mineral group is shown in Table 4. PC1 shows moderate eigenvector loading for reflectance bands 4 (0.470484) and 7 (0.404652); also in absorption band 6 (0.437957) while the highest and positive value (0.650457) is recorded in band 1 (absorption band). PC2 shows high and positive eigenvector loading in band 1 (0.650457) whereas in band 7, a high but negative value is observed (-0.75681). PC4 showed moderately low and negative eigenvector loadings for bands 1, 6 and 7 and a high and positive value in band 4 (0.876846). In PC3, low and positive eigenvector loading is noticed in band 1 (0.304497), very low and negative value in band 4 (-0.09378), very high and positive eigenvector loading in band 6 (-0.80856) and approximately high and positive value in band 7 (0.494687). Most hydroxyl minerals have their diagnostic absorption in band 6 (Fig 2) and PC with the largest contrast between the diagnostic absorption and reflectance bands should be a good candidate PC for mapping hydroxyl mineral group. PC3 has the highest contrast in the diagnostic absorption band for hydroxyl mineral group - band 6 and in reflectance – band 7 making it a choice single band PC for hydroxyl mineral discrimination.

RGB Composite generated from the sign inverted PC2 for ferric iron-oxide, PC3 for the hydroxyl bearing and sign inverted PC4 for the silica rich minerals is given in Fig 5.

Table 4 Eigenvector matrix of principal components analysis on ASTER data targeting silica rich, ferric and hydroxyl bearing materials. *(Choice PC in red; Absorption bands in red and reflectance band in Black)*

S/N	Target mineral group	Eigenvector	Band 10	Band 11	Band 12	Band 14
1	**Silica**	PC 1	-0.43107	-0.4618	-0.48358	-0.60586
		PC 2	0.244556	0.44728	0.343224	-0.78888
		PC 3	0.795894	-0.05372	-0.60134	-0.04536
		PC 4	**-0.34774**	**0.764066**	**-0.53548**	**0.092437**

2	**Ferric Oxide/hydroxide**	**Eigenvector**	**Band 1**	**Band 3**	**Band 4**	**Band 5**
		PC 1	0.648059	0.426218	0.467597	0.423922
		PC 2	**0.498953**	**0.323076**	**-0.31535**	**-0.73974**
		PC 3	0.474714	-0.41879	-0.65305	0.415681
		PC 4	-0.32513	0.733875	-0.50541	0.316667
3	**Hydroxyl bearing mineral**	**Eigenvector**	**Band 1**	**Band 4**	**Band 6**	**Band 7**
		PC 1	0.650457	0.470484	0.437957	0.404652
		PC 2	0.608072	0.031492	-0.23768	-0.75681
		PC 3	**0.304497**	**-0.09378**	**-0.80856**	**0.494687**
		PC 4	-0.33828	0.876846	-0.31293	-0.13703

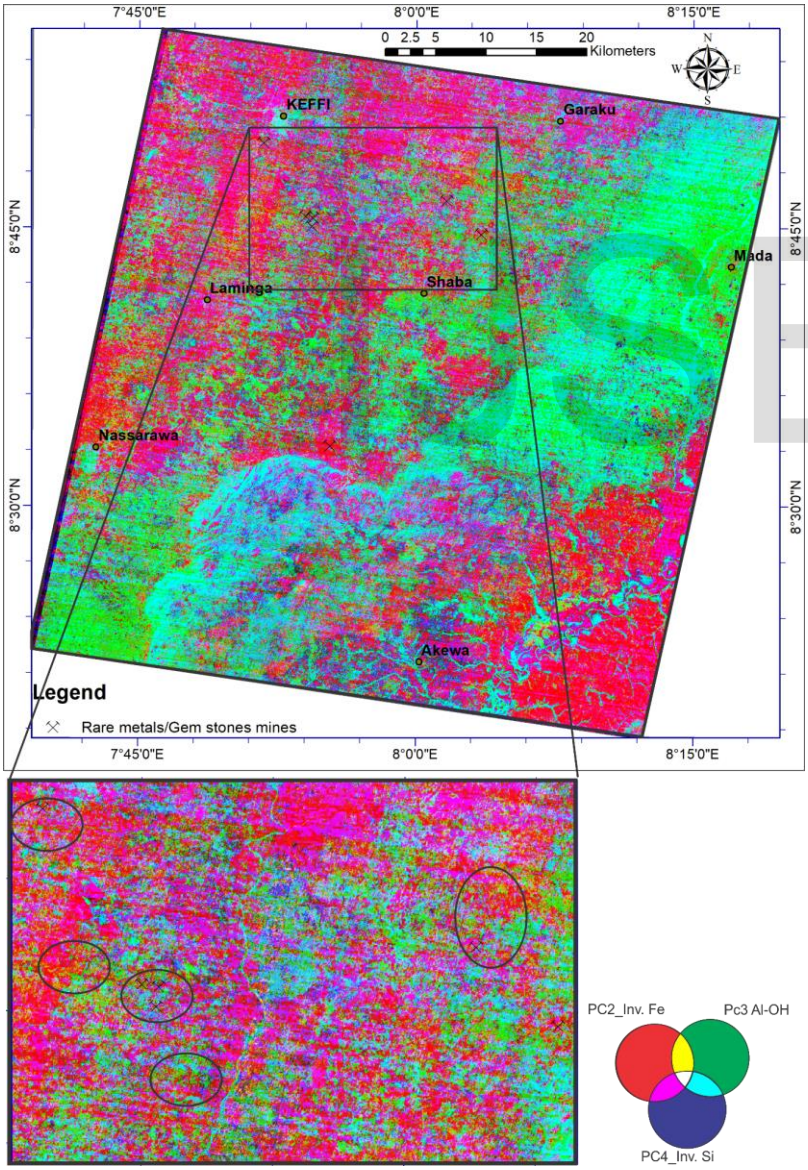

Fig. 5(a): RGB Composite of Fe_PC2_inv, Ka_PC3 and Si_PC4inv. 2% linear stretch applied to composite (b):Subset showing mineralized areas in purple with taints of yellow. Most of the known mines fall around these areas.

5.0 Conclusions

Band ratio techniques and PCA has been successfully used to discriminate the mineralised zones within the study area. RGB composite of B4/B3, (B7+B5)/B6 and B13/B10 respectively mapped the mineralised zones in whitish shades. This coincided with the area with complex pegmatites associated with the gemstone and rare metal mineralisation within the study area.

Feature oriented Principal Component analysis carried out mapped the ferric oxide in PC2 with sign inversion, Al-OH bearing material in PC3 and Silica rich material in sign inverted PC4. Result of the composite generated also agrees with the image from band ratio composite.

Acknowledgements

The authors are thankful to Tertiary Education Trust Fund (TETFund) for funding this research (IBR/2016-2017/79PS) work. Credit is also due to US Geological Survey (USGS) for access to the ASTER data used for this work.

References

1. F. J. Testa, C. Villanueva, D. R. Cooke, and L. Zhang, "Lithological and Hydrothermal Alteration Mapping of Epithermal, Porphyry and Tourmaline Breccia Districts in the Argentine Andes Using ASTER Imagery", Remote Sensing, vol. 10, **(2018)**, pp. 203-213; doi:10.3390/rs10020203
2. A.B. Pour and M. Hashim, "Identification of hydrothermal alteration minerals for exploring of copper deposit using ASTER data, SE Iran", Journal of Asian Earth Sciences, vol. 42, **(2011)**, pp. 1309-1323.
3. G. Ferrier, and G. Wadge, "Application of imaging spectrometry data to mapping alteration zones associated with gold mineralisation in southern Spain", International Journal of Remote Sensing, vol. 17, **(1996)**, pp. 331–350.
4. T. Cudahy, Satellite ASTER Geoscience Product Notes for Australia. Australian ASTER Geoscience Product Notes, Version 1, 7th August, (**2012)** – CSIR0 ePublish No. EP-30-07-12-44.
5. M. Haest, T. Cudahy, C. Laukamp, and S. Gregory, "Quantitative mineralogy from visible to shortwave infrared spectroscopic data - I. Validation of mineral abundance and composition products of the Rocklea Dome channel iron deposit in Western Australia". Economic Geology, vol. 107, **(2012)**, pp. 209 – 228.
6. T. J. Cudahy, M. Jones, M. Thomas, C. Laukamp, M. Caccetta, R. D. Hewson, A. D. Rodger, and M. Verrall, "Next Generation Mineral Mapping: Queensland Airborne HyMap and Satellite ASTER Surveys 2006-2008". CSIRO report P2007/364, **(2008)**. 153 pages.
7. L. C. Rowan, J. C. Mars, and C. J. Simpson, "Lithologic mapping of the Mordor, NT, Australia ultramafic complex by using the Advanced Spaceborne Thermal Emission and Reflection Radiometer (ASTER)". Remote Sensing of Environment, vol. 99, **(2005),** pp. 105–126.
8. R. D. Hewson, T. J. Cudahy, S. Mizuhiko, K. Ueda, A. J. Mauger, "Seamless geological map generation using ASTER in the Broken Hill–Curnamona province of Australia". Remote Sensing of Environment, vol. 99, **(2005)**, pp. 159–172.
9. L. C. Rowan and J. C. Mars, "Lithologic mapping in the Mountain Pass, California area using Advanced Spaceborne Thermal Emission and Reflection Radiometer (ASTER) data". Remote Sensing of Environment, vol. 84, **(2003)**, pp. 350–366.
10. T. J. Cudahy, and E. R. Ramanaidou, "Measurement of the hematite-goethite ratio using field VNIR spectrometry in channel iron deposits, Western Australia". Australian Journal of Earth Sciences, vol. 44, no. 4, **(1996)**, pp. 411-421.
11. A. P. Crosta, C. R. De Souza Filho, F. Azevedo and C. Brodie, "Targeting key alteration minerals in epithermal deposits in Pantagonia, Argentina, using ASTER imagery and principal component analysis", International Journal of Remote Sensing, vol. 24, **(2003)**, p. 4233 – 4240. DOI: 10.1080/0143116031000152291
12. N. S. Öztan and M. L. Süzen, "Mapping evaporate minerals by ASTER", International Journal of Remote Sensing, vol. 32, no. 6, **(2011)** pp. 1651-1673, DOI: 10.1080/01431160903586799.
13. R. Black, R. Caby, A. Moussine- Pouchkine, R. Bayer, J. M. Betrand, M. M. Boullier, J. Fabre, and A. Resquer, "Evidence for late Precambrian plate tectonics in West Africa". Nature, vol. 278, **(1979)**, pp. 223-227.
14. R. Caby, J. M. L. Betrand, and R. Black, "Pan-African ocean closure and continental collision in the Hogger-Iforas segment, central sahara. In: Kroner, A. (ed) Precambrian plate tectonics", Elsevier Amsterdam. **(1981)**, pp. 407-437.

15. S. S. Dada, "Crust-forming ages and proterozoic crustal evoluton in Nigeria: a reappraisal of current interpretations", Precambrian Research., vol. 87, **(1998)**, pp. 65-74.
16. P. McCurry, "The geology of the Precambrian to lower Paleozoic rocks of Nigeria". In: Kogbe, C.A. (ed) Geology of Nigeria. Elizaberthan, Lagos, Nigeria. (**1976)**, pp. 15-31.
17. M. A. Rahaman, and D. Ocan, "On Relationship in the Precambrian Migmatitic Gneiss of Nigeria", Journal of Mining and Geolology., vol. 15, **(1978)**, pp. 23-32.
18. M. O. Oyawoye, "The basement complex of Nigeria". In: Dessauvagie TFJ, Whiteman AJ (eds) African geology. Ibadan University Press, **(1972)**, pp 66–102.
19. J. D. Falconer, "The Geology and Geography of Northern Nigeria". Macmillan, London, **(1911)**, 135pp.
20. K. M. Goodenough, P. A. J. Lusty, N. M. W. Roberts, R. M. Key and A. Garba, "Post-collisional Pan-African granitoids and rare metal pegmatites in western Nigeria: Age, petrogenesis, and the 'pegmatite conundrum". Lithos, vol. 200, (2014), pp. 22-34.
21. G. Ferrier, K. White, G. Griffiths, R. Bryant, and M. Stefouli, "The mapping of hydrothermal alteration zones on the island of Lesvos, Greece, using an integrated remote sensing data set", International Journal of Remote Sensing, vol. 23, **(2002)**, pp. 341–356.
22. A. Moghtaderi, F. Moore and A. Mohammadzadeh, "The application of advanced space-borne thermal emission and reflection (ASTER) radiometer data in the detection of alteration in the Chadormalu paleocrater, Bafq region, Central Iran", Journal of Asian Earth Sciences, vol. 30, **(2007)**, pp. 238–252.
23. G. R. Hunt, "Spectral signatures of particulate minerals in the visible and near infrared", Geophysics., vol. 42, **(1977)**, pp. 501–513.
24. A. Kalinowski, and S. Oliver, "ASTER Mineral Index Processing Manual". Remote Sensing Applications Geoscience Australia. **(2004)**, 37p.
25. A. Singh and A. Harrison, "Standardised principal components", International Journal of Remote Sensing, vol. 6, **(1985)**, pp. 883–896.
26. Q. Chang, L. Jing and A. Panahi, "Principal component analysis with optimum order sample correlation coefficient for image enhancement". International Journal of Remote Sensing, vol. 27, **(2006)**, pp. 3387–3401.
27. R. P. Gupta, R. K. Tiwari, V. Saini and N. Srivastava, "A simplified approach for interpreting principal component images". Advances in Remote Sensing, vol. 2, **(2013)**, pp. 111-119. DOI:http://dx.doi.org/10.4236/ars.2013.22015.
28. C. Sabine, "Remote sensing strategies for mineral exploration". In Remote Sensing for the Earth Sciences – Manual of Remote Sensing, vol. 3, 3rd edn, A. Rencz Ed., **(1999)**, New York: Wiley.
29. A. P. CROSTA, and J. M. MOORE, "Enhancement of Landsat Thematic Mapper imagery for residual soil mapping in SW Minas Gerais State Brazil: a prospecting case history in greenstone belt terrain". In Proceedings of the 9th Thematic Conference on Remote Sensing for Exploration Geology, Pasadena, CA, **(1989)**, pp. 1173–1187 (Ann Arbor: Environmental Research Institute of Michigan).
30. W. P. Loughlin, "Principal components analysis for alteration mapping". Photogrammetric Engineering and Remote Sensing, vol. 57, **(1991)**, pp. 1163–1169.
31. L. Bastianelli, G. D. Bela, and I. L. Tars, "Alteration mapping: a case study in mid-south Bolivia". In Proceedings of the 9th Thematic Conference on Geologic Remote Sensing, Pasadena, CA, **(1993)**, pp. 1133–1144 (Ann Arbor: Environmental Research Institute of Michigan).
32. E. J. M. Carranza, and M. Hale, "Mineral imaging with Landsat Thematic Mapper data for hydrothermal alteration mapping in heavily vegetated terrain". International Journal of Remote Sensing, vol. 23, **(2002)**, pp. 4827–4852.
33. J. W. Boardman, and R. O. Green, "Exploring the Spectral Variability of the Earth as Measured by AVIRIS in 1999". Summaries of the Ninth Annual JPL Airborne Geosciences Workshop. Jet Propulsion Laboratory Special Publication 18, (2000), 10p.